The Astrophysical Journal, 619:931–938, 2005 February 1

THE WAVELENGTH DEPENDENCE OF INTERSTELLAR EXTINCTION FROM 1.25 TO 8.0 μm USING GLIMPSE DATA

R. Indebetouw,[1,2] J. S. Mathis,[1] B. L Babler,[1] M. R. Meade,[1] C. Watson,[1] B. A. Whitney,[3] M. J. Wolff,[3] M. G. Wolfire,[4] M. Cohen,[5] T. M. Bania,[6] R. A. Benjamin,[7] D. P. Clemens,[6] J. M. Dickey,[8] J. M. Jackson,[6] H. A. Kobulnicky,[9] A. P. Marston,[10] E. P. Mercer,[6] J. R. Stauffer,[11] S. R. Stolovy,[11] and E. Churchwell[1]

Received 2004 June 17; accepted 2004 October 8

ABSTRACT

We determine and tabulate $A_{[\lambda]}/A_K$, the wavelength dependence of interstellar extinction, in the Galactic plane for 1.25 μm $\leq \lambda \leq$ 8.0 μm along two lines of sight: $l = 42^\circ$ and 284°. The first is a relatively quiescent and unremarkable region; the second contains the giant H II region RCW 49, as well as a "field" region unrelated to the cluster and nebulosity. Areas near these Galactic longitudes were imaged at *J*, *H*, and *K* bands by 2MASS and at 3–8 μm by *Spitzer* for the GLIMPSE Legacy program. We measure the mean values of the color excess ratios $(A_{[\lambda]} - A_K)/(A_J - A_K)$ directly from the color distributions of observed stars. The extinction ratio between two of the filters, e.g., A_J/A_K, is required to calculate $A_{[\lambda]}/A_K$ from those measured ratios. We use the apparent *JHK* magnitudes of giant stars along our two sight lines and fit the reddening as a function of magnitude (distance) to determine A_J kpc^{-1}, A_K kpc^{-1}, and A_J/A_K. Our values of $A_{[\lambda]}/A_K$ show a flattening across the 3–8 μm wavelength range, roughly consistent with the extinction measurements derived by Lutz and coworkers for the sight line toward the Galactic center.

Subject headings: dust, extinction — infrared: ISM

1. INTRODUCTION

Extinction by interstellar dust affects most astronomical observations. The wavelength dependence of interstellar extinction has been studied extensively, but it is not well understood in the 3–9 μm region (Draine 2003). The Infrared Array Camera (IRAC; Fazio et al. 2004) on board the *Spitzer Space Telescope* is in the process of vastly increasing the number of observations in this wavelength region. Understanding the effects of dust extinction in the IRAC bands is important to properly interpret these observations.

The wavelength dependence of interstellar extinction, A_λ, is commonly treated as "universal" in the infrared because it apparently varies far less between different sight lines than does extinction in the optical and ultraviolet. Many authors have concluded that A_λ is a power law ($A_\lambda \propto \lambda^{-\beta}$) between $\sim$1 and $\sim$4 μm. Martin & Whittet (1990) found $\beta = 1.8$ in the diffuse interstellar medium (ISM), as well as in the outer regions of the ρ Oph and Tr 14/16 clouds. Other authors have fitted values between 1.6 and 1.8 (Draine 2003). A value of $\beta = 1.8$ implies that $E_{J-H}/E_{H-K} = (A_J - A_H)/(A_H - A_K) = 1.8 \pm 0.1$ (the value changes slightly depending on the exact filters and source spectrum). Deep surveys of specific dark clouds in the *JHK* bands have revealed significantly different color ratios, ranging from $E_{J-H}/E_{H-K} = 1.47 \pm 0.06$ for luminous southern stars (He et al. 1995) to 2.08 ± 0.03 in the Coalsack (Racca et al. 2002, and references therein). At wavelengths approaching 9.7 μm, A_λ is dominated by absorption by the Si—O stretching mode of interstellar silicates. There is uncertainty in the wavelength dependence of interstellar extinction between the power-law regime at 1–2 μm and the discrete silicate feature. Observations of H_2 rovibrational lines in Orion (Bertoldi et al. 1999; Rosenthal et al. 2000) are consistent with continuation of the power law to $\lesssim$4 μm, but their uncertainties are too large to constrain the extinction at longer wavelengths. *Infrared Space Observatory* (*ISO*) observations of hydrogen recombination lines by Lutz et al. (1996) toward the Galactic center show a flattening of A_λ in the region 3 μm $\lesssim \lambda \lesssim$ 9 μm. Lutz (1999) confirms this flattening using more recombination lines toward the Galactic center and also shows evidence of extra mid-IR extinction toward external galaxies.

The Galactic Legacy Infrared Mid-Plane Survey Extraordinaire (GLIMPSE; see Benjamin et al. 2003), a *Spitzer* Legacy program, uses IRAC to obtain photometric images of the inner Galactic plane in four filters ([3.6], [4.5], [5.8], and [8.0] μm) simultaneously. By combining stellar photometry of the GLIMPSE images with the 2MASS[12] point-source catalog, we can sample A_λ/A_K at seven wavelength points [λ] in the near-IR (NIR, defined in this paper as 1.2–8.0 μm): 1.240, 1.664, 2.164,

[1] Department of Astronomy, University of Wisconsin at Madison, 475 North Charter Street, Madison, WI 53706.
[2] Current address: Department of Astronomy, University of Virginia, P.O. Box 3818, Charlottesville, VA 22903-0818.
[3] Space Science Institute, University of Colorado, 1540 30th Street, Suite 23, Boulder, CO 80303-1012.
[4] Astronomy Department, University of Maryland, College Park, MD 20742-2421.
[5] Radio Astronomy Lab, University of California, Berkeley, 601 Campbell Hall, Berkeley, CA 94720.
[6] Institute for Astrophysical Research, Boston University, 725 Commonwealth Avenue, Boston, MA 02215.
[7] Physics Department, University of Wisconsin at Whitewater, 800 West Main Street, Whitewater, WI 53190.
[8] Department of Astronomy, University of Minnesota, 116 Church Street, SE, Minneapolis, MN 55455.
[9] Department of Physics and Astronomy, University of Wyoming, P.O. Box 3905, Laramie, WY 82072.
[10] ESTEC/SCI-SA, Postbus 299,2200 AG Noordwijk, Netherlands.
[11] *Spitzer* Science Center, California Institute of Technology, MS 314-6, Pasadena, CA 91125.

[12] This publication makes use of data products from the Two Micron All Sky Survey (2MASS), which is a joint project of the University of Massachusetts and the Infrared Processing and Analysis Center/California Institute of Technology, funded by the National Aeronautics and Space Administration and the National Science Foundation. Throughout this paper we refer to the 2MASS K_s filter as *K*.

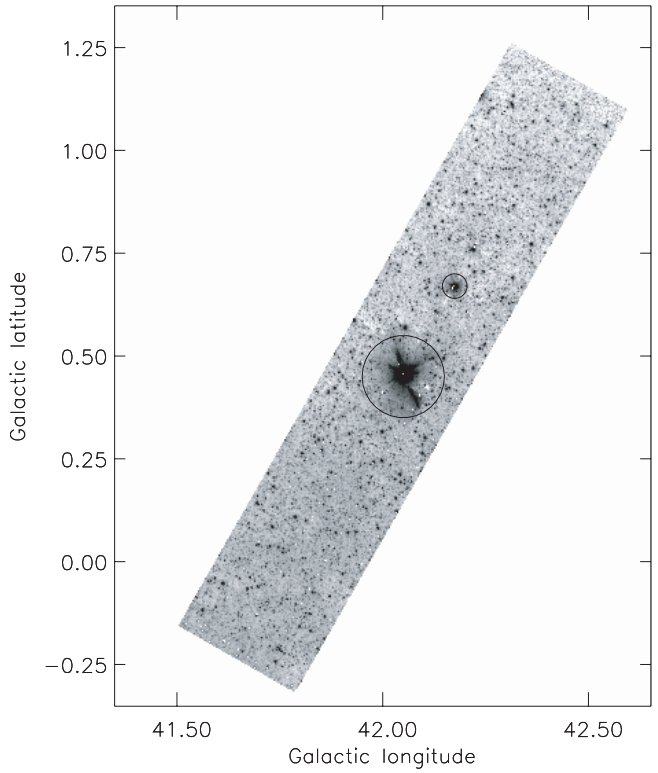

FIG. 1.—GLIMPSE 3.6 μm image of the region near $l = 42^\circ$ used in this study. The bright spots in the center are highly saturated stars; the regions around them are excluded from GLIMPSE photometry (*circles*).

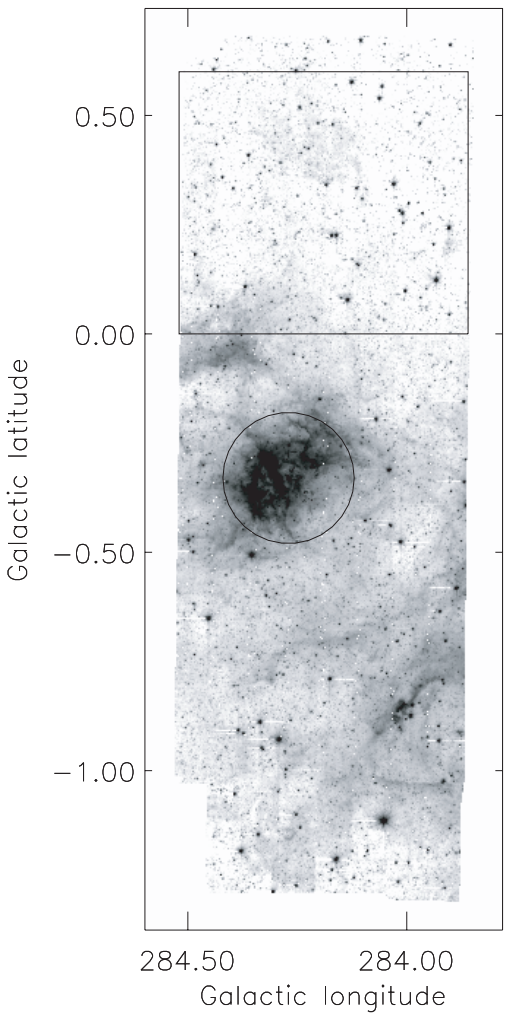

FIG. 2.—GLIMPSE 3.6 μm image of the region near $l = 284^\circ$ used in this study. The region near the giant H II region RCW 49 is marked with a circle, and the "field" region away from nebulosity, star formation, and significant CO emission (Dame et al. 2001) is marked with a square.

3.545, 4.442, 5.675, and 7.760 μm. The adopted wavelengths are the isophotal wavelengths of the 2MASS and IRAC filters convolved with a K2 III star, which we use as our standard probe of extinction along the line of sight (see discussion below).[13]

We describe the data and their basic reduction in § 2, and our method of measuring color excess ratios $E_{[\lambda]-K}/E_{J-K}$ in § 3. Section 4 discusses the conversion of these colors to A_λ and issues related to interpretation. In § 5 we summarize and tabulate our recommended relative extinction values for the GLIMPSE/IRAC bands.

2. PHOTOMETRY OF GLIMPSE DATA

This paper uses stellar photometry in the Galactic plane obtained from two subsets of GLIMPSE data. The first data set (Fig. 1), $0.^\circ33 \times 1.^\circ72$ centered on $(l,\ b) = (42^\circ,\ 0.^\circ5)$, was obtained during in-orbit checkout (IOC; 2003 October, PID 631). The imaged region is a fairly unremarkable part of the Galactic plane. The second data set (Fig. 2), $283.^\circ9 \leq l \leq 284.^\circ5$ and $-1.^\circ3 \leq b \leq 0.^\circ7$, was obtained for the purposes of observing strategy validation (OSV; 2003 December, PID 195). The region contains the giant H II region RCW 49 and its associated massive cluster (Churchwell et al. 2004 and references therein).

Basic reduction of IRAC images was performed by the *Spitzer* Science Center (SSC) Pipeline (ver. 8.9.0 at $l = 42^\circ$ and ver. 9.0.1 at $l = 284^\circ$). Positional accuracies are better than $1''$ (Werner et al. 2004). Point-source FWHM resolution of IRAC data ranges from $\simeq 1.''6$ at [3.6] to $\simeq 1.''9$ at [8.0]. The data were further processed by the GLIMPSE pipeline (Benjamin et al. 2003). Point sources were found and fluxes extracted from each frame using a version of DAOPHOT (Stetson 1987), modified to be more robust in regions of rapidly varying high background (B. L. Babler et al. 2005, in preparation). To calculate stellar colors, we adopt zero-magnitude flux densities of 277.5, 179.5, 116.6, and 63.1 Jy for the four IRAC bands (Fazio et al. 2004). For this present study, we culled the catalog to include only those sources with signal-to-noise greater than 10 in each band. The magnitude to which stars are well measured in all bands is limited by the [5.8] and [8.0] bands that typically contain high diffuse backgrounds (the calculated uncertainty for flux density is higher if the local background is higher). At the limiting magnitude of 12.5, photometric uncertainties are less than 0.08, 0.09, 0.12, and 0.14 mag in the [3.6], [4.5], [5.8], and [8.0] bands, respectively. If we only require detections at wavelengths shorter than 5 μm (e.g., for measuring the extinction at [4.5]), then we can include sources as faint as 14 mag at [3.6] and [4.5], with photometric uncertainties greater than 0.15 mag. The flux calibration was checked by comparing extracted fluxes

[13] Filter wavelengths depend on the spectrum of the source, but differences are small and have little effect on our results—for example, the flat-spectrum isophotal wavelengths for 2MASS are 1.235, 1.662, and 2.159 μm, and the SSC-provided isophotal wavelengths for IRAC are 3.535, 4.502, 5.650, and 7.735 μm.

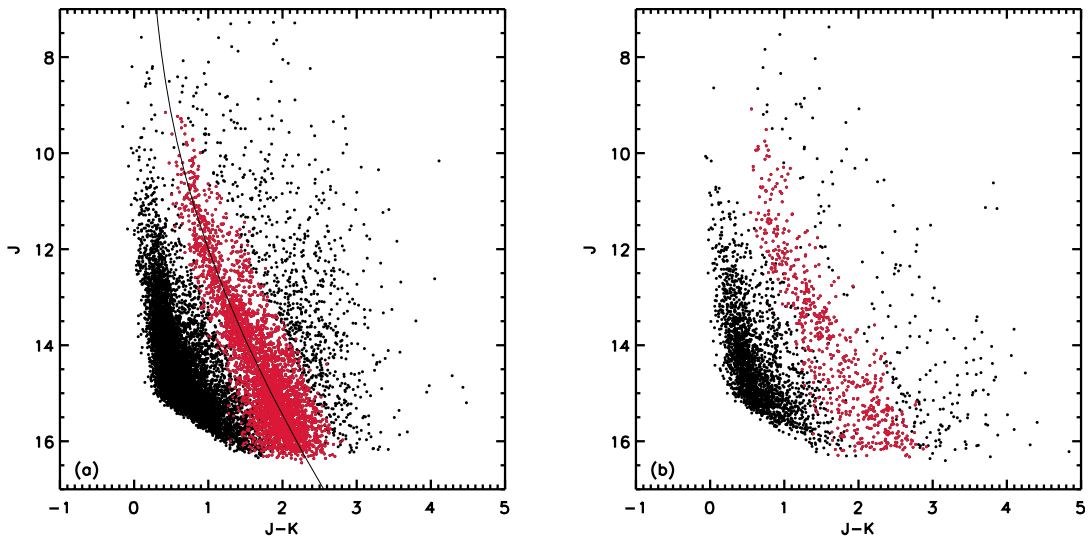

FIG. 3.—(*a*) Color-magnitude diagram for field sources (away from RCW 49) near $l = 284^\circ$. Features common in Galactic sight lines are the vertically extended concentrations of points at $J - K \simeq 0.5$ corresponding to dwarf stars and at $1 \lesssim J - K \lesssim 2$ (*red points*) corresponding to mostly red clump giants (see text and Drimmel et al. 2003). We can isolate the red clump giants and fit their distribution (best fit is the overplotted line) to determine A_J/A_K and the absolute extinction with distance (J mag kpc^{-1}; see text for discussion of uncertainties). (*b*) The plot for the region around the giant H II region RCW 49—interestingly, the spread of red clump giants is very weak faintward of $J \simeq 14$, $J - K \simeq 1.75$. This is likely caused by an opaque interstellar cloud, and if that cloud is associated with RCW 49, we can estimate the distance to be 5 ± 1 kpc.

with modeled fluxes for five early A-type dwarf stars—these agreed to within 7% for all IRAC bands (Cohen et al. 2003; Kurucz 1993). Detections of the same source in different images and different filters were band-merged (cross-identified), and detections were additionally merged with the 2MASS point-source catalog to provide *JHK* fluxes for many sources. Tests of band-merging in crowded fields using synthetic data show that fewer than 0.5% of sources are falsely cross-identified down to the flux limits used in this work.

The data segment at $l = 42^\circ$ was imaged before the telescope was fully focused. The point-spread function (PSF) is thus different from that in subsequent IRAC data. We do not expect the precision of our photometry to suffer since in the GLIMPSE pipeline the PSF is constructed from the data for each epoch of data collection. We did not assess the flux calibration independently for the IOC data as we did for the OSV data, but we do not see any gross errors, nor do we expect any, because the standard *Spitzer* calibration strategy was determined before launch. Results in this paper are derived from relative colors, which are insensitive to zero-point issues in the photometry.

3. MEASUREMENT OF EXTINCTION

We determine the relative extinction $A_{[\lambda]}/A_K$ using photometry of approximately 10,000 stars ([λ] refers to the three 2MASS and four IRAC filters). Two different processes are required. First, we measure color excess ratios $E_{[\lambda]-K}/E_{J-K}$ by fitting the loci of a population of stars in color-color diagrams. Second, we need a single ratio of extinctions, say A_J/A_K, determined or estimated independently. The calculation of $A_{[\lambda]}/A_K$ from $E_{[\lambda]-K}/E_{J-K}$ follows simply

$$\frac{A_{[\lambda]}}{A_K} = \left(\frac{A_J}{A_K} - 1\right)\frac{E_{[\lambda]-K}}{E_{J-K}} + 1. \quad (1)$$

Various observational studies and dust theories find a range of A_J/A_K between 2.25 and 2.75 (Cardelli et al. 1989; Fitzpatrick 1999; Draine 2003). We determine the ratio A_J/A_K directly from our data by fitting the locus of red clump giants in a color-magnitude diagram. Both steps in our process are only possible using a fairly sensitive, uniform, large-area survey such as 2MASS or GLIMPSE.

3.1. *Determining A_J/A_K*

We determine the extinction ratio A_J/A_K by fitting the locus of reddened K giants in color-magnitude space. These stars are bright enough ($M_J \lesssim -1.5$, e.g., López-Corredoira et al. 2002) that 2MASS and GLIMPSE can observe them to great distances through the Galactic plane. The intrinsic luminosity and color distributions of red clump K giants are determined by the evolution of stars from the main sequence and the initial mass function, is fairly narrow ($\pm \lesssim 0.5$ mag) and should not change with distance. We use the wavelength-independent effect of distance on apparent magnitude (the $1/d^2$ change in flux), together with the wavelength-dependent effect of extinction, to determine the average extinction per unit distance and thus the absolute ratio of extinctions, A_J/A_K.

In Figure 3, the apparent J magnitudes of the field stars near $l = 284^\circ$ are plotted against their $J - K$ colors. This color-magnitude diagram shows features common along Galactic sight lines, in particular those at longitudes where the disk component dominates over the bulge component. A vertically extended concentration of points at $J - K \sim 0.5$ are predominantly main-sequence dwarfs at a range of distances (8365 sources in this particular plot). A second concentration (3560 sources) extending from $J \simeq 12$, $J - K \simeq 1$ to $J \simeq 16$, $J - K \simeq 2$ are predominantly giants. Distance spreads the distribution vertically in the figure; extinction moves a statistically uniform sample of stars vertically and horizontally by an amount proportional to distance, provided that the dust per unit distance is approximately constant. We note that the dwarf and giant sequences are not parallel—this is expected if the distribution of dwarfs is affected not only by interstellar reddening at faint J but also by the addition of intrinsically faint, numerous cool dwarfs. The absolute magnitudes of giants, by contrast, are dominated by the red clump giants of early K type, with fairly narrow color and luminosity distributions.

There are no intrinsically faint local stars to be added to the giant sequence at faint J; instead, we have a population of intrinsically similar beacons, spread along the line of sight. The distinct red clump feature is discussed and exploited to probe Galactic structure by López-Corredoira et al. (2002) and further used by Drimmel et al. (2003) to calculate the amount of extinction along certain Galactic lines of sight. The 859 points redward of the giants in Figure 3 are probably mostly intrinsically red asymptotic giant branch stars.

We perform a four-variable minimization to fit the curved red giant branch star locus and determine the amount of extinction per unit distance. The curve can be written parametrically as a function of distance d:

$$J = J_0 + 5\log(d/10\text{ pc}) + c_J(d/10\text{ pc}), \quad (2)$$

$$J - K = J_0 - K_0 + (c_J - c_K)(d/10\text{ pc}), \quad (3)$$

where c_J is the average extinction per unit distance in the J band, assumed constant for a given line of sight. We select the red giant clump stars (Fig. 3, *red points*) by their *JHK* apparent magnitudes and colors, and use the IDL program *amoeba* to minimize the sum of the squared distances between each data point and the line defined by equation (3).

If we wish only to determine the ratio $c_J/c_K = A_J/A_K$, then J_0 and K_0 can be determined by best fit for the population of giants along the particular sight line. We get the same results for c_J/c_K whether J_0 and K_0 are fixed at the values suggested by López-Corredoira et al. (2002) for a K2 III ($M_K = -1.65$, $H - K = 0.75$, intrinsic spread of 0.3 mag in the population) or allowed to vary. We varied the region of the sky, the color selection criteria for red giant branch stars, the initial guess for the four parameters, and the degree of robustness in the fit algorithm (iteratively rejecting high-σ outliers). The range in fit coefficients is larger than the numerically calculated σ for each fit, and we use that larger range as our quoted uncertainty. The uncertainty in the extinction per unit distance c_J is larger than in the ratio c_J/c_K, because it depends on assuming the absolute J and K magnitudes of the red clump.

We fitted the locus of red clump giants in all possible *JHK* color-magnitude diagrams ($J - K$ vs. J, $H - K$ vs. K, etc.). Our derived ratios are $A_J/A_K = 2.5 \pm 0.2$, $A_H/A_K = 1.55 \pm 0.1$, and $A_J/A_H = 1.65 \pm 0.1$. As noted above, we also measure the average magnitudes of extinction per kpc along this line of sight: $c_J = 0.35 \pm 0.15$ mag kpc^{-1}, $c_H = 0.25 \pm 0.1$ mag kpc^{-1}, and $c_K = 0.15 \pm 0.1$ mag kpc^{-1}. These are about 1 σ higher than numbers often used for the average Galactic disk, $c_V \simeq 0.7$ mag kpc^{-1} or $c_J \simeq 0.2$ mag kpc^{-1}. Examining the color-magnitude diagrams also reveals two regions of high extinction along the line of sight toward $l = 284^\circ$: at $J \simeq 12.7$, $J - K \simeq 1.3$ and $J \simeq 14.3$, $J - K \simeq 1.7$. The extinction of the more distant cloud is so high toward the RCW 49 giant H II region that few red clump giants are seen beyond it (see Fig. 3). If that cloud is associated with RCW 49, as seems reasonable, then we can estimate the distance to be 5 ± 1 kpc, independently of any other distance measurement. Finally, it is more difficult to fit the giant branch toward $l = 42^\circ$ because of greater contamination by asymptotic giant branch (AGB) stars and the bulge red giants at magnitudes fainter than $J \simeq 14$, but we find the same ratios of $A_J/A_H/A_K$ within uncertainties.

3.2. *Determining Color Excess Ratios*

We measure each color excess ratio $E_{[\lambda]-K}/E_{J-K}$ by fitting the locus of a population of stars in a color-color diagram. The color excess $E_{[\lambda]-K}$ is defined as the difference between a star's observed and intrinsic color. The excess for a particular star is proportional to the amount of dust along the sight line to that star, but ratios of color excesses reveal the wavelength dependence of extinction. If one plots colors $[\lambda] - K$ versus $J - K$, the slope of the source distribution is the color excess ratio $E_{[\lambda]-K}/E_{J-K}$, as illustrated in Figure 4.

In each region of the sky, we fitted a line to the stellar colors $([\lambda] - K)/(J - K)$ of only the giant stars (selected by their *JHK* magnitudes and plotted in red in Fig. 3). Extremely red sources (at the bottom of the first four panels in Fig. 4) likely have nonphotospheric emission from circumstellar dust; these outliers must be excluded from measurement of interstellar dust *extinction*, because the dust *emission* has a different wavelength dependence and appears as nonphysical extra reddening. A small number of highly evolved (AGB) stars can also fall in the excluded region because of absorption bands in their atmospheres. We calculated fits using several different algorithms and used the differences in results to estimate our uncertainties; the simplest fit performed was a linear regression weighted by uncertainties in both axes. In addition to fitting all sources and fitting only red clump giants, we tried arbitrarily excluding sources with extreme red excesses (e.g., with $([\lambda] - K) < -0.3$ $(J - K) - 0.65$). We also used a robust algorithm that iterates the fit, rejecting high-σ outliers. This also has the effect of excluding some of the extreme red excess sources.

Figure 5 shows the measured color excess ratios $E_{[\lambda]-K}/E_{J-K}$ plotted as a function of λ^{-1} for the RCW 49 giant H II region, the field near $l = 284^\circ$, and the field near $l = 42^\circ$. The plotted values are listed in Table 1, along with average values. The uncertainties are a combination of variation in fit results depending on the exact part of the sky, stellar population, and fit algorithm, calculated uncertainty of the fit coefficients, and errors in GLIMPSE and 2MASS photometry (in order of decreasing significance). There is good agreement among the excess ratios measured in all three regions, although the data are from very different directions in the Galactic plane. More extensive interpretation is possible after conversion of the measured color excess ratios into relative extinction $A_{[\lambda]}/A_K$, as discussed in the next section.

An alternative method for measuring the color excess ratios due to interstellar extinction that is not dependent on the intrinsic stellar color distribution is described by Kenyon et al. (1998). The method consists of comparing a selection of stars presumed to be mostly behind an extincting cloud with a selection of stars not extinguished by the cloud ("off-cloud"). Instead of plotting colors (e.g., $H - K$), one plots all possible color *differences* $([\lambda] - K)_i - ([\lambda] - K)_j$ versus $(H - K)_i - (H - K)_j$ (where i indexes all "cloud" stars and j all off-cloud stars). If the stellar color distributions are statistically the same in the two samples, the color difference plot is a tight distribution extended along the extinction vector. As before, the slope of that distribution is the color excess ratio $E_{[\lambda]-K}/E_{J-K}$. We calculated the wavelength dependence of extinction from GLIMPSE and 2MASS data using the RCW 49 region as cloud and the region away from the H II region to the north as off-cloud. The results ($E_{[\lambda]-K}/E_{J-K} = 0.36 \pm 0.02$, -0.31 ± 0.02, -0.36 ± 0.02, -0.40 ± 0.03, and -0.37 ± 0.02, for H, [3.6], [4.5], [5.8], and [8.0], respectively) are the same within the line-fitting uncertainties as the values listed in Table 1 that were obtained from the simpler method described above.

We have discussed ratios of color excesses $E_{[\lambda]-K}/E_{J-K}$. The use of J and K in the denominator is convenient because we determine A_J/A_K from the color-magnitude relation (see § 3.1), but the $A_{[\lambda]}/A_K$ we derive is independent of this choice. For completeness, we fitted other color excess ratios and found that

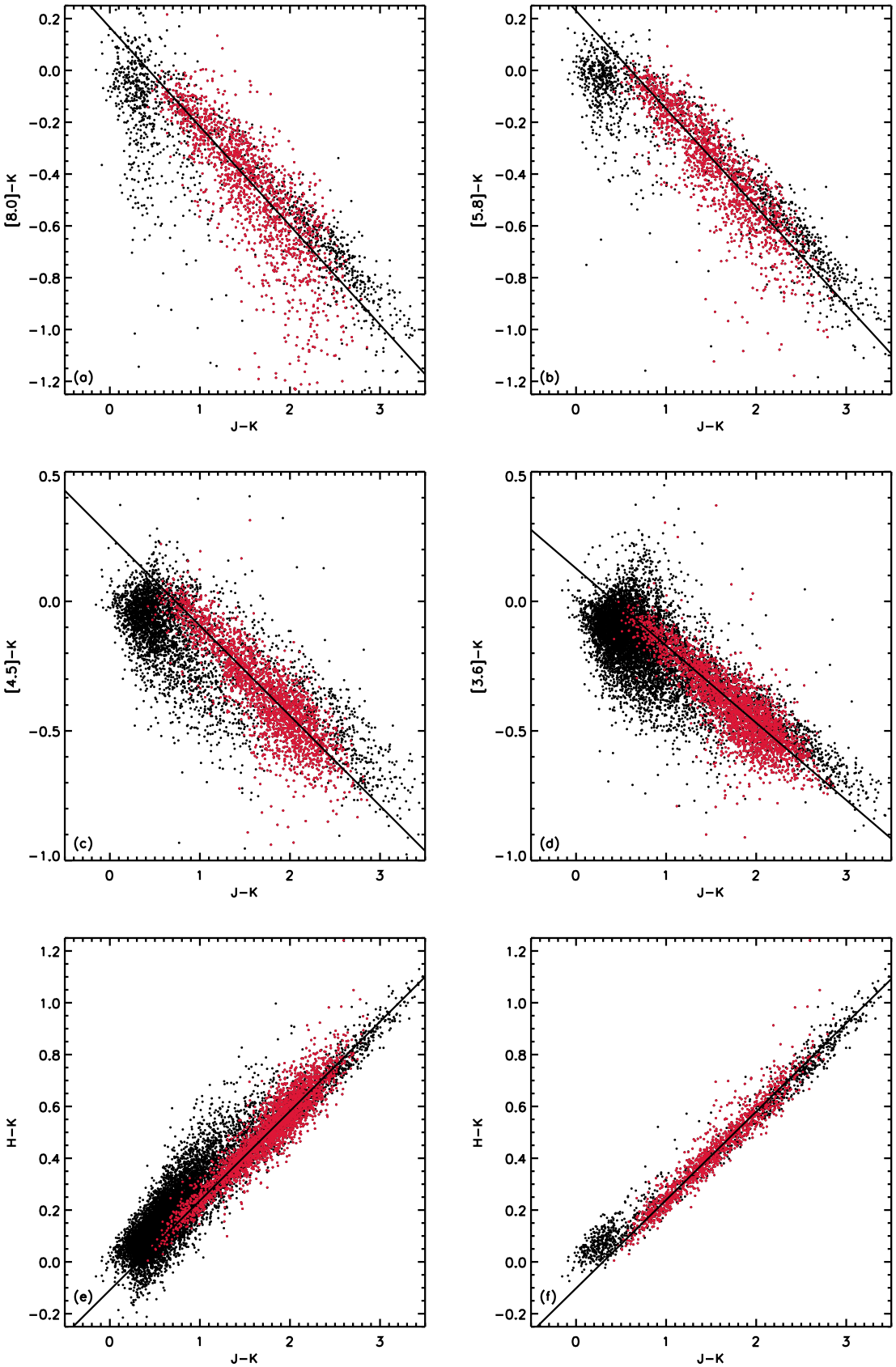

FIG. 4.—Color-color diagrams of sources detected by GLIMPSE and 2MASS in the "field" ($b > 0$, away from known H II regions) near $l = 284^{\circ}$. The slope of a line fitted to each source distribution is the color excess ratio $E_{[\lambda]-K}/E_{J-K}$. We fitted only the red clump giants, selected by their location in the $J, J-K$ color-magnitude diagram and plotted here in red. The first four panels, (*a*)–(*d*), show source colors $J-K$ vs. $[\lambda]-K$ for the four IRAC bands $[\lambda]$. Panels (*d*) and (*e*) show $J-K$ vs. $H-K$ for sources with high-quality fluxes in the *JHK* bands, and for only those sources with high-quality fluxes in all seven filters, respectively. If one fits only the latter stars, the slopes change by $\lesssim$5%, and this has been included in error estimates. The dominant source of scatter in these plots is variation in the intrinsic colors of stars ($\simeq \pm 0.3$ mag López-Corredoira et al. 2002). Sources with nonphotospheric emission from circumstellar dust (traditionally called "infrared excess" sources) appear as extreme outliers, e.g., at the bottom of (*a*), $[8.0]-K$ vs. $J-K$.

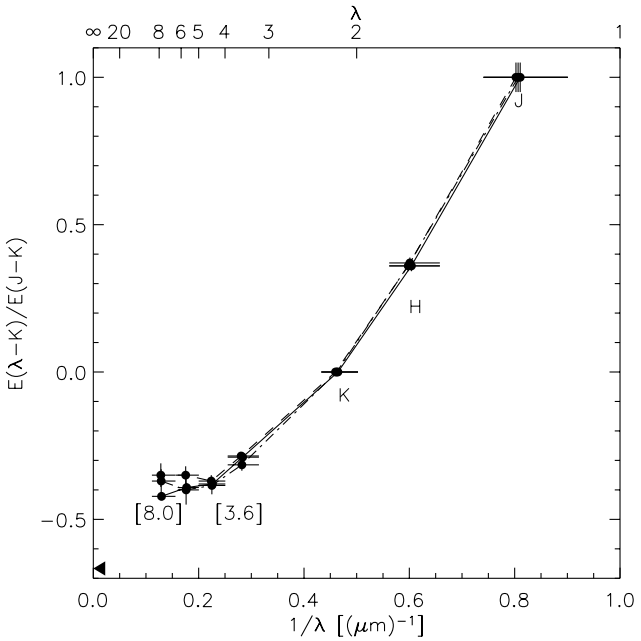

FIG. 5.—Color excess ratio $E_{[\lambda]-K}/E_{J-K}$ plotted as a function of $1/\lambda$, for the RCW 49 region (*dot-dashed line*) and for the "field" near $l = 284^\circ$ (*solid line*), and for the "field" near $l = 42^\circ$ (*dashed line*). Error bars on the field curves are smaller than for RCW 49, and comparable to the sizes of the points. Horizontal bars indicate the filter widths and the fact that we have only sampled the wavelength dependence of interstellar extinction at those discrete filters. The filled arrowhead is discussed below.

the resulting ratios did not change within uncertainty—for example,

$$\frac{E_{[4.5]-K}}{E_{J-K}} = 0.35 \pm 0.02,$$

$$\left(\frac{E_{[4.5]-[3.6]}}{E_{[3.6]-K}} + 1\right)\left(\frac{E_{[3.6]-K}}{E_{J-K}}\right) = (0.16 \pm 0.03 + 1)(0.30 \pm 0.02) = 0.35 \pm 0.07.$$

4. THE WAVELENGTH DEPENDENCE OF INTERSTELLAR EXTINCTION A_λ

4.1. *Determination of* $A_{[\lambda]}/A_K$

With color excess ratios from the slopes of color-color plots (§ 3.2) and A_J/A_K determined from the color-magnitude relation of giants (§ 3.1), equation (1) yields $A_{[\lambda]}/A_K$. The presence of enough data points from 2MASS and GLIMPSE to measure A_J/A_K directly from our data is very important to this study. Color excess ratios are sensitive only to *changes* in the extinction with wavelength. Without A_J/A_K, we would have to extrapolate $E_{[\lambda]-K}/E_{J-K}$ in Figure 5 from K band to $\lambda^{-1} = 0$; the intercept of that extrapolated curve is $-A_K/(A_J - A_K) = 1/(1 - A_J/A_K)$. Although this extrapolation is a commonly used procedure, it is difficult to perform accurately and questionable because of the absorption features of silicates peaking at 9.7 and 18 μm. The arrowhead at the bottom left of Figure 5 shows the value of $1/(1 - A_J/A_K)$ using our values measured as described in § 3.1. By assuming a power law through the *JHK* relative extinctions (effectively an extrapolation to $\lambda^{-1} = 0$), Martin & Whittet (1990) estimated $A_J/A_K = 2.7$. This value requires the intercept in Figure 5 to be -0.59. Our intercept derived from fitting the red clump giants is at -0.67.

Figure 6 shows the derived $A_{[\lambda]}/A_K$ for the field stars at $l = 284^\circ$ (*solid diamonds*), for $l = 42^\circ$ (*open diamonds*), and for the dust surrounding RCW 49 (*solid circles*). The uncertainties are a combination of uncertainty in determining A_J/A_K, variation in fit results depending on the exact part of the sky, stellar population, and fit algorithm, calculated uncertainty of the fit coefficients, and errors in GLIMPSE and 2MASS photometry (in order of decreasing significance). There is good agreement between the three determinations of $A_{[\lambda]}/A_K$, in two very different directions of the Galactic plane, and even toward a giant H II region.

A simple fit to the average $A_{[\lambda]}/A_K$ in the three regions is given by

$$\log[A_\lambda/A_K] = 0.61(\pm 0.04) - 2.22(\pm 0.17)\log(\lambda) + 1.21(\pm 0.23)[\log(\lambda)]^2, \quad (4)$$

where λ is in μm. The fit curve is plotted along with the data points in Figure 6 and is recommended for use between 1.25

TABLE 1
IRAC EXTINCTION $A_{[\lambda]}/A_K$

Location	J 1.240 μm[a]	H 1.664 μm	K 2.164 μm	[3.6] 3.545 μm	[4.5] 4.442 μm	[5.8] 5.675 μm	[8.0] 7.760 μm
				$E_{[\lambda]-K}/E_{J-K}$			
RCW 49	1.0	0.37 ± 0.02	0.0	-0.31 ± 0.03	-0.38 ± 0.03	-0.40 ± 0.05	-0.37 ± 0.04
$l = 284^\circ$	1.0	0.35 ± 0.02	0.0	-0.30 ± 0.02	-0.35 ± 0.02	-0.38 ± 0.02	-0.38 ± 0.03
$l = 42^\circ$	1.0	0.36 ± 0.02	0.0	-0.29 ± 0.02	-0.37 ± 0.02	-0.35 ± 0.03	-0.35 ± 0.04
Average	1.0	0.36 ± 0.02	0.0	-0.30 ± 0.01	-0.37 ± 0.02	-0.38 ± 0.04	-0.37 ± 0.04
				$A_{[\lambda]}/A_K$			
RCW 49	2.50 ± 0.15	1.56 ± 0.06	1.00	0.53 ± 0.07	0.42 ± 0.09	0.40 ± 0.14	0.45 ± 0.11
$l = 284^\circ$	2.50 ± 0.15	1.54 ± 0.05	1.00	0.57 ± 0.05	0.43 ± 0.07	0.41 ± 0.07	0.37 ± 0.07
$l = 42^\circ$	2.50 ± 0.15	1.54 ± 0.06	1.00	0.57 ± 0.06	0.45 ± 0.07	0.48 ± 0.09	0.48 ± 0.11
Average	2.50 ± 0.15	1.55 ± 0.08	1.00	0.56 ± 0.06	0.43 ± 0.08	0.43 ± 0.10	0.43 ± 0.10

[a] The adopted wavelengths are the isophotal wavelengths of the 2MASS and IRAC filters convolved with a K2 III star—see § 1.

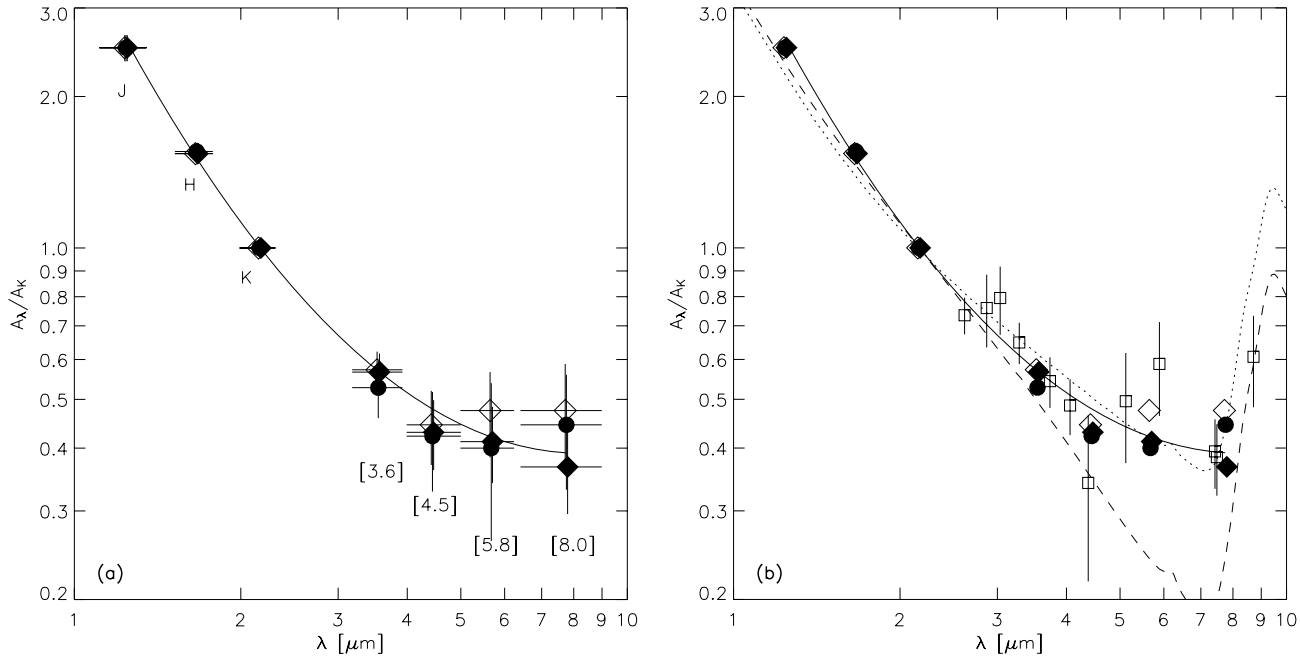

FIG. 6.—(*a*) Derived relative extinction values for RCW 49 (*solid circles*), the field near $l = 284^\circ$ (*solid diamonds*), and the field near $l = 42^\circ$ (*open diamonds*). The open and solid diamonds coincide at $\lambda = 3.5$ μm. The lines show fits (see eq. [4]) to the mean field (*solid line*) and RCW 49 (*dot-dashed line*). Horizontal bars indicate the filter widths and the fact that we have only sampled the wavelength dependence of interstellar extinction at those discrete filters. (*b)* The measurements of Lutz et al. (1996) have been added (*squares with error bars*), as well as theoretical curves from Weingartner & Draine (2001) for $R_V = 5.5$ (their case A is shown by a dashed line, and their case B is shown by a dotted line).

and 7.75 μm. (Note that a simple power-law extinction curve with $\beta = 1.8$ has coefficients of 0.60, -1.8, and 0.0.)

For historical reasons, the filter to which A_λ is compared is usually taken to be A_V, and our extinction measurements are presented as $A_{[\lambda]}/A_K$. In contrast to NIR extinction, optical extinction ($\lambda < 1$ μm) is known to vary significantly among sight lines (Cardelli et al. 1989; Fitzpatrick 1999); the variation is well characterized by a single parameter, $R_V = A_V/E_{B-V}$. The variation of A_V/A_K is beyond the scope of this paper, but $A_V/A_K \sim 8.8$ for $R_V = 3.1$ and $\sim$7.5 for $R_V = 5$ (Cardelli et al. 1989). In general, the lack of variation of the extinction curve throughout the NIR among various environments (in comparison to its strong dependence on R_V in the optical/ultraviolet) suggests that it may not be possible to estimate A_V/A_K for our data set from NIR observations alone.

4.2. *Comparison with Previous Measurements and Discussion*

Previous measurements of the wavelength and spatial dependence of interstellar extinction in this wavelength regime differ. It is important to note that the measured excesses at IRAC wavelengths ($\lambda > 3$ μm) lie above the curve extrapolated from $\lambda < 3$ μm (see Fig. 5). This implies a source of extinction in the IRAC wavelength regime that is in excess of the power-law wavelength dependence exhibited by a grain model tuned to UV-optical extinction observed in the diffuse ISM (e.g., Weingartner & Draine 2001, case A). Our measurements reject a pure power-law extinction curve by more than 4 σ at 6 μm. Lutz et al. (1996) and Lutz (1999) observed the Galactic center with the Short Wavelength Spectrometer on *ISO* in the interval 2.4–45 μm, using recombination lines of hydrogen to provide intrinsic flux ratios. They converted their reddening values to A_λ/A_K by assuming a theoretical value of A_K/A_V from Draine (1989). Figure 6 shows that the Lutz et al. (1996) values are very similar to those presented in this work but show more scatter.

Our values of $A_{[\lambda]}/A_K$ are consistent with Lutz et al. (1996) and Lutz (1999) in spite of the large differences in method and sight lines. Their color excess ratios pertain to the line of sight to the Galactic center, while our $l = 42^\circ$ sight line probes only the outer 30% of that Galactocentric distance and $l = 284^\circ$ is confined to approximately the solar circle. The path to the Galactic center contains $A_V \sim 5$–10 mag of extinction from molecular clouds (which may exhibit different extinction than the diffuse ISM; see discussion and references in Whittet et al. 1997), out of a total $A_V \sim 25$ mag. The molecular fraction of the ISM in our regions is at present unknown at adequate spatial resolution; low-resolution ^{12}CO (Dame et al. 2001) measurements suggest that only a few magnitudes of the observed $A_V \sim 10$–15 may be from molecular clouds. Finally, using nebular emission lines to provide the extinction assumes that the extinction is uniform over the $14'' \times 20''$ aperture of the *ISO* spectrometer, whereas using stellar photometry probes a pencil beam along each line of sight. Our measurements are consistent with Lutz et al. (1996) despite all of these differences in methodology and circumstance.

The similarities of the wavelength dependence of extinction for our two very different Galactic longitudes and, to within larger errors, toward the Galactic center (Lutz et al. 1996; Lutz 1999), is remarkable. This suggests an almost universal extinction law in the infrared. Even toward the massive star-forming region RCW 49 the extinction is very similar to that observed in the "field" regions.

It is useful to estimate the extent to which the [8.0] IRAC band is affected by the silicate feature that peaks at 9.7 μm. Most stars emit the peak of their emission far shortward of the IRAC wavelengths, and their emission in the Rayleigh-Jeans limit weights the filter response toward shorter effective wavelengths. The *Spitzer* Science Center–provided isophotal wavelength is 7.735 μm, at which the silicate opacity is less than 10% of that at 9.7 μm (e.g., Jaeger et al. 1994, 1998). The *ISO* spectra

of heavily obscured objects in Gibb et al. (2004) show 8 μm fluxes that seem little affected by silicate absorption. Nevertheless, the filter is broad, and silicate absorption in the diffuse ISM appears consistent with an FWHM of 2.3 μm, possibly wider in molecular clouds (Roche & Aitken 1984; Bowey et al. 1998). Convolution of the IRAC filter profile with a source emitting a Rayleigh-Jeans spectrum and with a Gaussian absorption feature at 9.7 μm shows that the silicate feature could have as much as a 20% effect on the filter flux. Studies of individual objects (especially those with circumstellar dust) could show more variation in the [8.0] extinction with source spectral shape than the average ISM results presented here. The effect of the silicate feature on the [5.8] IRAC band is negligible.

The ratio of polarization to extinction is an important diagnostic of the nature of grains. Consider aligned grains of a particular type of material. At a particular wavelength, both extinction and polarization are integrals of similar optical constants over the size distribution of the grains. Both polarizations and extinctions at both 4 and 8 μm have been measured in two molecular clouds: GL 2591 and the BN object in Orion (see Martin & Whittet 1990 for observations and references). Because of atmospheric opacity, there are no measurements between these wavelengths. In GL 2591, $p(4\ \mu\mathrm{m})/p(8\ \mu\mathrm{m}) \sim 2.5$; in BN, $p(4\ \mu\mathrm{m})/p(8\ \mu\mathrm{m}) \sim 2.0$. The silicate strengths are also similar; $p(10\ \mu\mathrm{m})/p(8\ \mu\mathrm{m}) \sim 3.7$ for GL 2591 and 4.3 for BN. Equation (4) shows that our measured extinction ratio $A(4\ \mu\mathrm{m})/A(8\ \mu\mathrm{m}) \sim 1.32$, significantly below the 4 μm/8 μm polarization ratio of either object. The wavelength dependence of the polarization outside of the ice band is similar for these two clouds but differs significantly from our measured wavelength dependence of extinction, suggesting that *the grains providing the 8 μm extinction are different from the silicates at 10 μm and those providing 4 μm extinction* (carbonaceous?), and that *they are not as well aligned*. The alternative to this conclusion is that the dust within Orion BN and GL 2591 has a wavelength dependence of extinction significantly different from the dust observed by GLIMPSE.

5. CONCLUSIONS

We have measured the wavelength dependence of interstellar extinction in the 1.25–8.0 μm region by combining GLIMPSE and 2MASS observations. The values calculated for two very different directions in the Galactic plane are remarkably similar. Even near the giant H II region RCW 49, extinction is not significantly different. It may be possible to study variations of extinction with Galactic longitude using the entire GLIMPSE survey, expected to be complete by early in the year 2005. Since the values of E_{J-H}/E_{H-K} in the Galactic plane are somewhat higher than at higher Galactic latitude, there may be differences in the extinction at IRAC wavelengths as well.

The similar derived behavior of the extinction along several different sight lines suggests that our relative extinction values $A_{[\lambda]}/A_K$ may be generally applicable. Our average extinction measurements may be used to correct GLIMPSE and other IRAC data in the Galactic plane. These values are provided in Table 1, and the simple formula of equation (4) provides an analytical fit of simple functional form.

We acknowledge the invaluable assistance of Stephan Jansen for maintaining the GLIMPSE computing network. We thank the referee, Bruce Draine, for comments and discussion that improved the paper. Support for this work, part of the *Spitzer Space Telescope* Legacy Science Program, was provided by NASA through contract numbers (institutions) 1224653 (University of Wisconsin at Madison), 1225025 (Boston University), 1224681 (University of Maryland), 1224988 (Space Science Institute), 1242593 (University of California, Berkeley), 1253153 (University of Minnesota), 11253604 (University of Wyoming), 1256801 (University of Wisconsin at Whitewater) by the Jet Propulsion Laboratory, California Institute of Technology, under NASA contract 1407. This research made use of MONTAGE, funded by NASA's Earth Science Technology Office, Computational Technologies Project, under Cooperative Agreement Number NCC5-626 between NASA and the California Institute of Technology. We acknowledge use of data products from the Two Micron All Sky Survey, a joint project of the University of Massachusetts and the Infrared Processing and Analysis Center/California Institute of Technology, funded by NASA and the NSF. *Spitzer* data used in this paper are from PID 195 (multiple AORs) and from PID 631, AOR 0007283968.

REFERENCES

Benjamin, R. A., et al. 2003, PASP, 115, 953
Bertoldi, F., Timmermann, R., Rosenthal, D., Drapatz, S., & Wright, C. M. 1999, A&A, 346, 267
Bowey, J. E., Adamson, A. J., & Whittet, D. C. B. 1998, MNRAS, 298, 131
Cardelli, J. A., Clayton, G. C., & Mathis, J. S. 1989, ApJ, 345, 245
Churchwell, E., et al. 2004, ApJS, 154, 322
Cohen, M., Megeath, S. T., Hammersley, P. L., Martín-Luis, F., & Stauffer, J. 2003, AJ, 125, 2645
Dame, T. M., Hartmann, D., & Thaddeus, P. 2001, ApJ, 547, 792
Draine, B. T. 1989, in Proc. 22 ESLAB Symp. Infrared Spectroscopy in Astronomy, ed. B. Kaldeich (ESA SP-290; Noordwijk: ESA), 93
———. 2003, ARA&A, 41, 241
Drimmel, R., Cabrera-Lavers, A., & López-Corredoira, M. 2003, A&A, 409, 205
Fazio, G., et al. 2004, ApJS, 154, 10
Fitzpatrick, E. L. 1999, PASP, 111, 63
Gibb, E. L., Whittet, D. C. B., Boogert, A. C. A., & Tielens, A. G. G. M. 2004, ApJS, 151, 35
He, L., Whittet, D. C. B., Kilkenny, D., & Spencer Jones, J. H. 1995, ApJS, 101, 335
Jaeger, C., Molster, F. J., Dorschner, J., Henning, T., Mutschke, H., & Waters, L. B. F. M. 1998, A&A, 339, 904
Jaeger, C., Mutschke, H., Begemann, B., Dorschner, J., & Henning, T. 1994, A&A, 292, 641
Kenyon, S. J., Lada, E. A., & Barsony, M. 1998, AJ, 115, 252
Kurucz, R. 1993, CD-ROM 12, ATLAS9 Stellar Atmosphere Programs and 2 km/s grid (Cambridge: SAO)
López-Corredoira, M., Cabrera-Lavers, A., Garzón, F., & Hammersley, P. L. 2002, A&A, 394, 883
Lutz, D. 1999, in The Universe as Seen by *ISO*, ed. P. Cox & M. F. Kessler (ESA SP-427; Noordwijk: ESA), 623
Lutz, D., et al. 1996, A&A, 315, L269
Martin, P. G., & Whittet, D. C. B. 1990, ApJ, 357, 113
Racca, G., Gómez, M., & Kenyon, S. J. 2002, AJ, 124, 2178
Roche, P. F., & Aitken, D. K. 1984, MNRAS, 208, 481
Rosenthal, D., Bertoldi, F., & Drapatz, S. 2000, A&A, 356, 705
Stetson, P. B. 1987, PASP, 99, 191
Weingartner, J. C., & Draine, B. T. 2001, ApJ, 548, 296
Werner, M. W., et al. 2004, ApJS, 154, 1
Whittet, D. C. B., et al. 1997, ApJ, 490, 729